Accepted Manuscript

Silkworm silk fibers vs PEEK reinforced rubber luminescent strain gauge and stretchable composites

Luca Valentini, Silvia Bittolo Bon, Lorenzo Mussolin, Nicola Pugno

PII: S0266-3538(17)32086-9

DOI: 10.1016/j.compscitech.2017.12.031

Reference: CSTE 7019

To appear in: *Composites Science and Technology*

Received Date: 23 August 2017

Revised Date: 17 November 2017

Accepted Date: 28 December 2017

Please cite this article as: Valentini L, Bon SB, Mussolin L, Pugno N, Silkworm silk fibers vs PEEK reinforced rubber luminescent strain gauge and stretchable composites, *Composites Science and Technology* (2018), doi: 10.1016/j.compscitech.2017.12.031.

Silkworm silk fibers vs PEEK reinforced rubber luminescent strain gauge and stretchable composites

Luca Valentini[1]*, Silvia Bittolo Bon[1], Lorenzo Mussolin[2], Nicola Pugno**[3,4,5]

1 Civil and Environmental Engineering Department, University of Perugia, UdR INSTM, Strada di Pentima 4, 05100 Terni, Italy.

Tel: +39 0744 492924; E-mail: luca.valentini@unipg.it

2 Physics Department and SERMS Laboratory, University of Perugia, Strada di Pentima 4, 05100 Terni, Italy.

3 Laboratory of Bio-Inspired and Graphene Nanomechanics, Department of Civil, Environmental and Mechanical Engineering, University of Trento, Trento - Italy

4 School of Engineering and Materials Science, Queen Mary University of London, Mile End Road, London - United Kingdom.

5 Ket-Lab, Edoardo Amaldi Foundation, Italian Space Agency, via del Politecnico snc, I-00133 Roma, Italy.

Tel: +39 0461 282525; E-mail: nicola.pugno@unitn.it

Abstract

In the present study we demonstrate how the sensitive property of the constituent parts of silkworm silk fiber can be applied to the field of soft composite materials. It concerns the structural and intrinsic functional characteristics of silk vs. the macroscopic property and the realization of functional composites. Silk fiber reinforced silicone rubber (SR) composites have been fabricated with different fiber lengths. The key structural features of silk made of stiff nanocrystals, including hydrogen bonded β-strands and β-sheet nanocrystals, when embedded in a softer matrix demonstrate that the tensile strength as well as the stiffness of the composites are higher than those measured for SR reinforced with synthetic polyether-ether-ketone fibers. Moreover, the intrinsic luminescence of protein nanocrystals permits the direct observation of the deformation with accurate measurement of the strain in the composite. Based on the intrinsic properties of such natural hierarchical material, these findings will allow to transfer the engineering of composite materials, particularly, soft functional composites, to a new applications ranging from strain measurements in biological tissue to monitoring tool in structural composites.

Keywords: silkworm silk; composites; mechanical properties; luminescence.

Introduction

The unique mechanical properties, biocompatibility and adaptability in industrial processes of silkworm silk fibers have been integrated in bioengineering structures in which they serves as model of light-weight composites [1-5]. Silkworm cocoon is a by-product of a natural process to protect butterflies from environment and predators [6] and can be considered as a natural polymer composite consisting of continuous fibers with a length of about 1000 m and diameters of 10–30 µm, which are glued together by sericin [7,8]. Removing the sericin with different degumming methods [9,10], silkworm silk could be used as natural fiber in the composite industry replacing glass and carbon fibers [11].

Silkworm silk fiber is a hierarchical material where hydrogen bonded β-strands, β-sheet nanocrystals, and a hetero-nanocomposite of stiff nanocrystals embedded in a softer semi-amorphous phase assembles into macroscopic silk fibers. It follows that the large breaking stress of silkworm silk fibers can be explained according to the hierarchical structures of the crystal domain and network [12]. In view of their surprising strength, the utilization of silkworm silk fibers as reinforcement for polymer composites is gaining attention in different fields of applications [12]. Fiber reinforced composites are a class of materials of growing interests in multiple application such as areospace, biomaterials, and infrastructure. The common feature in all composites is the presence of an interphase. Many measurement techniques and measurement tools have been developed for the study of this crucial region in composite materials. The development of methods that permit the direct observation of the deformation during applied stress are needed and important in several fields of applications.

For example, biological tissues such as skin, tendons and muscles are flexible and are subjected to large deformations under mechanical loading. Silkworm silk is known to be a biocompatible material with absence of toxicity and immunogenicity in biological environments, moreover, silk is a natural protein polymer where the non-invasive optical assessment of β sheet content and

orientation can be obtained by non-invasive fluorescent patterns [12,13]; in this regard, recently, silk fibroin, a protein core fiber extracted from the silkworm *B. mori*, and rhodamine pigment were dispersed in a polymer medium for monitoring the mechanical response of tissues [13]. Silk fibroin was also used in the replacement of polymers in existing electronic and photonic devices for biomedical purposes [14-16]. Moreover, on the basis of the mechanochromism phenomenon (consisting of colour changing of a material under mechanical stress) reported by Ito and co-worker [17], other authors have successfully visualized the strain distribution and crack generation through mechanoluminescence [18]. Thus, interfacing silk with luminescent dyes has also been proposed as potential tool for fundamental studies of composite interfacial damage and as a structural monitoring tool when used as fiber sensor for composite structures [19].

Thus, the step forward in this direction consists in the realization of fiber reinforced composite that uses only the intrinsic functional properties of the fibers to observe macroscopic behaviours such the strain under applied stress without the addition of fluorescent dyes. The realization of a silk fiber composite as strain-gauge at best of our knowledge is not reported elsewhere and is challenging because combines the stiffness of the silk fiber with the variation of the luminescence pattern of the β-sheet nanocrystals when stretched.

In this work we produce silkworm silk fiber reinforced silicone rubber composites with different fiber lengths. We demonstrate that the stiffness and the tensile strength are superior to those measured for the analogous synthetic PEEK fiber reinforced composite and that the composite stiffness can be modelled starting from the well-known Cox model [20]. Finally, using degummed silkworm silk fibers we propose the use of silicone rubber/silkworm silk fibers composite to fabricate an optical strain gauge by using the luminescent emission intensity of the silk fibers embedded in the rubbery matrix to measure the deformation of the composite.

Experimental details

Commercial *B. mori* organic cocoons for face cleaning were degummed in hot water with natural detergent to obtain silk strands. The degummed cocoons were washed in clean water and then dried in air. The fibers were collected by hand. Monofilament polyether-ether-ketone (PEEK) fibers kindly supplied by Zyex Ltd. (fiber diameter ~100 µm) were also used for comparison purposes. Degummed silk fibers (with an average diameter ~ 12 µm) and PEEK fibers were cut with lengths varying from 300 mm to 10 mm.

For the morphological characterization, as received cocoons with a diameter of 3.5 mm as well as silk and PEEK fibers were glued onto a conducting carbon tape and sputter coated. The coated samples were observed with a field emission scanning microscopy.

Cocoon strips with a width of 10 mm and length of 35 mm were cut in the direction of the long axis. Silk and PEEK fibers were mounted on paper frames with 65mm gauge length. The tensile properties of the fibers were measured using a universal tensile testing machine (Lloyd Instr. LR30K) with a 50 N static load cell with a speed of $1mm*min^{-1}$. Three samples were tested.

Silk fibers were then characterized by FTIR-ATR, differential scanning calorimetry (DSC) and thermogravimetric analysis (TGA). FTIR-ATR (Jasco FTIR 615) spectra were performed in the spectral region of 500 to 4000 cm^{-1}. DSC measurements were performed with a Q200 (TA), in the temperature range 25–250°C and with a heating rate of 10°C/min. TGA was performed in a SII TG/DTA 6300 (Seiko) in the temperature range of 25–800 °C with a ramp rate of 10°C/min and a nitrogen flow. X-ray diffraction (XRD) experiments on unloaded and loaded silkworm silk fibers were conducted with an XRD diffractometer (Bruker) with a radiation source of Cu Kα and wavelength λ= 0.154 nm operating at 40 kV and 40 mA. The incidence angle (2θ) was fixed between 1° and 60° and the scan rate was 0.02°/s.

Crystal liquid rubber (CRISTAL RUBBER purchased from PROCHIMA®, density 1.04 g/cm^3) was used for composite casting with a cold cure by poly-addition. Silkworm silk fibers and PEEK fiber reinforced silicone rubbers composites have been fabricated with different fiber length by liquid mixing; silk or/and PEEK fibers were dispersed in liquid silicone rubber (~1%wt.) through the utilization of a magnetic stirrer (500 rpm for 3 h) to facilitate their dispersion. Then, we add to the rubber 10wt% of PT-CURE catalyst (purchased from PROCHIMA®, density 1.04g/cm^3). The poly-addition process was completed in an aluminum mold for 24 h at room temperature. For the composite tensile tests, a static load cell of 500 N was used and the guage length was about 70 mm with a speed of 10 mm*min^{-1}. Three samples for each composite were tested.

The luminescence spectroscopy on the SR/silkworm silk fiber composites was performed using a 300 W Xenon arc lamp as the source for monochromatic excitation radiation combined with a Cornerstone 260 monochromator. A short-pass filter was used in order to clean the source signal, with a cut-off frequency of 450 nm and a transmission coefficient of about 0% at 462 nm. The radiation emitted by the specimens was collected with a Cypher-H spectrometer, and analyzed with the BW-Spec software. The specimen was hold in order to have the excitation source perpendicular to the specimen surface.

After performing a dark scan to set the zero for the spectrometer, a first scan of the monochromator output radiation, which was previously set at 450 nm, has been performed. In order to avoid any unwanted radiation above 450 nm, a second scan was performed by placing the short-pass filter between the monochromator and the spectrometer probe. The filtered signal has been used as excitation source for the whole test. In order to account for any possible contribution to the radiation shift, except the one of the silk, a scan of a pure silicon specimen was performed, with no significant emission shift. After placing the SR/silkworm silk fiber composite in place, the excitation source wavelength was lowered in steps of 5 nm, recording the specimen output with the spectrometer on every step. The integration time, as well as the number of scans used for averaging

the measure to minimize noise have been changed to account for the low emission of the Xenon lamp in the shorter wavelengths. A dark scan has been performed every time one of the aforementioned parameter was changed, in order to reestablish the correct zero of the device. The luminescence intensity variation was monitored under mechanical loading by reaching the maximum value of the stretch ratio λ_{max} (where λ = final length/initial length, or L_f/L_i) and bringing the composite to the initial state from λ_{max} to 1.

Results and discussion

As received cocoons contain a single continuous silk strand (inset of Fig. 1a), which is deposited layer by layer in loops by the gyrating motion of the silkworm head; in each strand of silk, two parallel fibers are glued together by a gummy outer layer of sericin, as observed by FESEM image in Fig. 1a. The resulting degummed silk mat consists of individual fibers with a mean diameter of about 12 µm (Fig. 1b). Monofilament PEEK fiber morphology is also reported in Fig. 1c for comparison purposes.

FTIR-ATR spectrum obtained on degummed silk fiber mat (see supplementary data, Fig. S1), shows typical absorption bands at 1641 cm^{-1} and, 1632 cm^{-1}, corresponding to amide I structural conformation [21]. Other absorption bands were observed at 1530 cm^{-1} (amide II) and 1237 cm^{-1} (amide III), which are characteristic of the silk random coil and β-helix conformation [21]. The DSC thermograms for the degummed silk fibers (see supplementary data, Fig. S1) showed the endothermic peak at 204.6 °C is attributed to the molecular motion within the α-helix crystals [22,23]. Thermal stability of the silk fibers was also investigated by TGA analysis with the thermal degradation that appears at about 290°C, while the initial weight loss, below 100 °C, was due to water evaporation (Fig. S1).

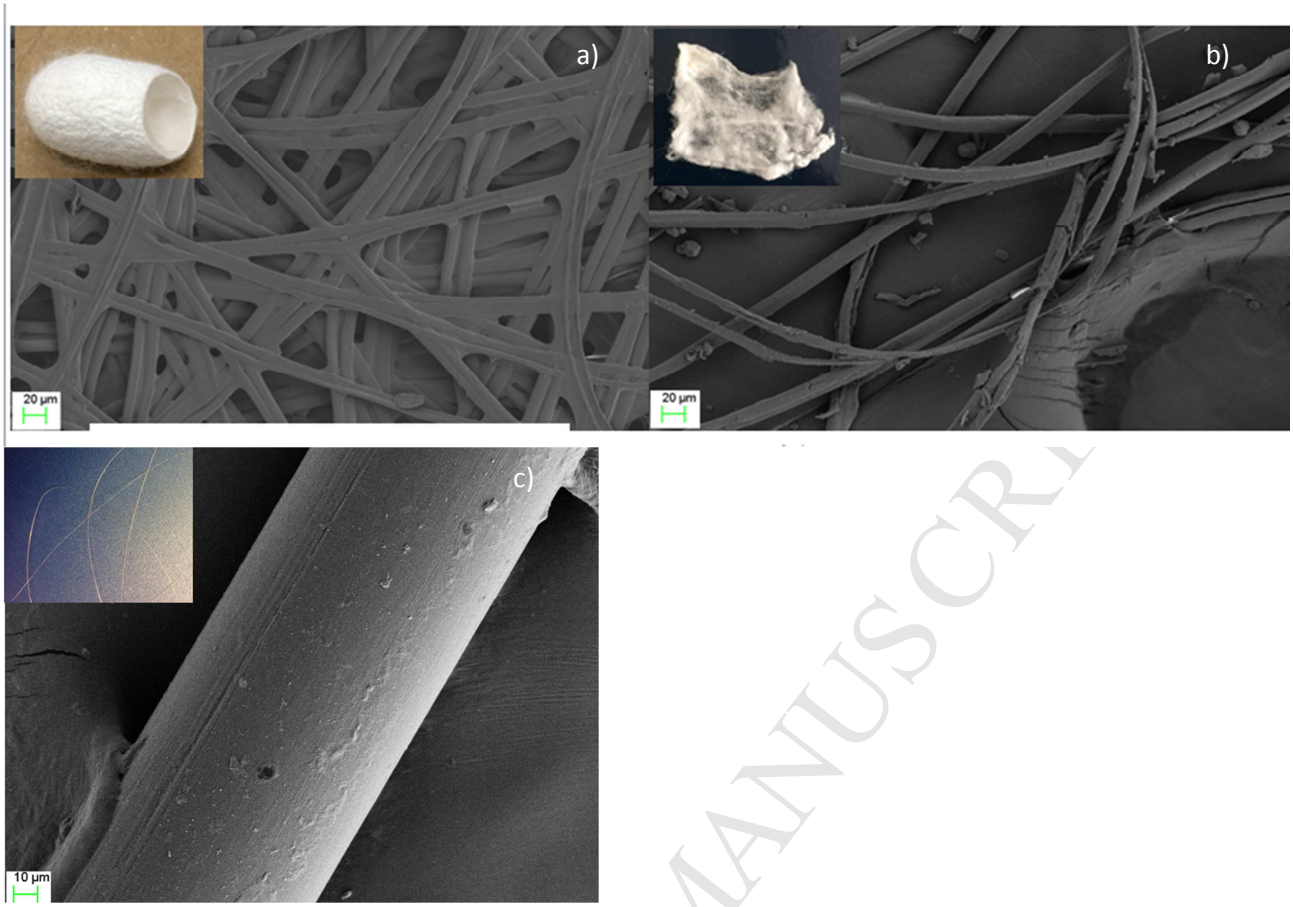

Figure 1. FESEM pictures of (a) silkworm cocoon, (b) degummed silk fibers and (c) monofilament PEEK fiber. Inset: photos of (a) a silkworm cocoon, (b) the degummed silk mat and (c) monofilament PEEK fiber.

The stress-strain behaviour of the silk cocoon has been investigated and compared with that of the silk fiber (Fig. 2) and the results were summarized in Table I. The tensile strength as well as the elastic modulus of the cocoons were found lower than those of the fiber; this is due to the fact that the elastic modulus controlled by the porosity [24,25]; this mechanism was investigated by Chen et al. [26] who proposed that the fibres sustain the load when the cocoon is stretched and the stress drops rapidly when the fibre bundles break. Thus, the weakness of the *B. mori* cocoons can be explained as a synergy effect between the high cocoon porosity and weak interlayer bonding [26]. In view of this model, the observed stress independence behaviour with strains above 0.5% in Fig. S3 of the supplementary data can be interpreted as an inter-fibre bonding break where the unbonded

fibres unravel from the non-woven structure. For the silk fibers, we also found (see Fig. S3) that fibers taken from different parts of the mat gave different stress strain curves and that the mechanical characteristics differ from those obtained by Chen et al. [26] in terms of elongation at break. This could be attributed both to the difference of the fibres during the worm spinning and to the degumming process adopted [9]. Finally it should be observed that the silk fiber is stiffer than the PEEK fiber (Table I) being the deviation standard on the tensile strength more narrow for these synthetic fibers.

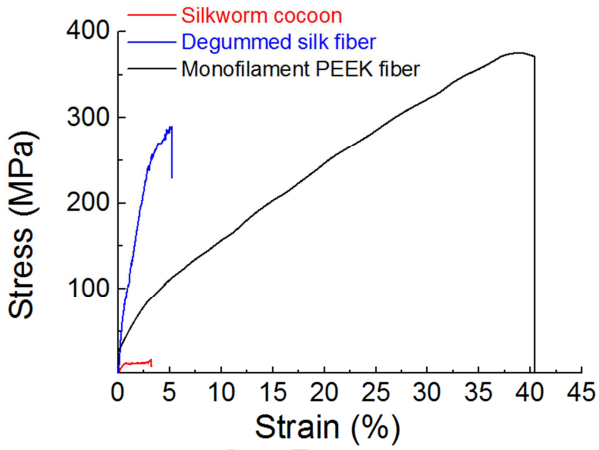

Figure 2. Tensile behaviour of silkworm cocoon (red curve), degummed silk fiber (blue curve) and monofilament PEEK fiber (black curve).

The main factors affecting the elastic modulus and the strength of fiber reinforced polymer composites are the content, the stiffness, the length and the orientation of the fibers [27]. In the general rule of mixture used for the determination of the stiffness and the strength of the composites new factors have to be taken in consideration as the fibers that are not continuous and long thus the load transfer is determined by the length efficiency factor η_{lE} [20] and that the fibers are randomly oriented, so the orientation factor η_{oE} has also to be introduced [28]. The Cox – Krenchel model modifies the rule of mixture as it follows

$$E_c = \eta_{lE} * \eta_{oE} * E_f * f + E_m * (1-f) \quad (1)$$

where E_c, E_f and E_m are the Young's modulus of the composite, fiber and matrix, respectively, *f* is the volume fraction fiber content (i. e. 0.6% see supplementary data) and

$$\eta_{lE} = 1-\tanh(\beta*l/2)/(\beta*l/2) \quad (2)$$

whit β equal to

$$\beta=(1/r)*(E_m/E_f*(1-\nu)*(\ln(\pi/4f))^{\wedge 1/2}) \quad (3)$$

where l is te fiber length, r is the fiber diameter and ν is the Poisson's ratio of the matrix.

The orientation factor, η_{oE}, as defined by Krenchel [29] is 1/5 for 3D randomly oriented fibers, 3/8 for random 2D mat, 1/2 for bidirectional (0°-90°) fibers and 1 for fibers oriented along the stretching direction.

Provided the values of the fiber and matrix stiffness (see Table I), the geometrical measurements of the fiber dimensions, the stiffness of SR/silkworm silk fibers composites is compared with that of technological SR/PEEK fibers composites as shown in Figs. 3a and 3b. From the stiffness modelling curves, the assumption of 3D random orientation factor results in a good agreement with the experimental data for both fiber reinforced composites without any best fitting procedure.

Table I. Mechanical characteristics of the tested specimens. For the composites, the fiber length is also indicated.

Samples	Young modulus (MPa)	Tensile strength (MPa)	Elongation at break (%)	Toughness modulus (MPa)
SR	0.4 ± 0.04	1.2 ± 0.1	325 ± 32	1.95 ± 0.14
Silkworm silk cocoon	2000 ± 500	8.0 ± 1.6	3.0 ± 0.5	0.12 ± 0.02
Silkworm silk fiber	12000 ± 2400	278 ± 70	5.0 ± 0.7	6.8 ± 1.4
SR/silkworm silk fibers (300 mm)	4.0 ± 1	2.0 ± 0.4	115 ± 34	1.15 ± 0.40
SR/silkworm silk fibers (100 mm)	3.6 ± 0.8	1.5 ± 0.3	102 ± 31	0.77 ± 0.23
SR/silkworm silk fibers (10 mm)	3.0 ± 0.8	0.8 ± 0.2	35 ± 8	0.14 ± 0.03
PEEK fiber	3550 ± 355	371 ± 37	40 ± 4	74.2 ± 7.4
SR/PEEK fibers (300 mm)	1.5 ± 0.4	1.6 ± 0.5	265 ± 53	2.12 ± 0.63
SR/PEEK fibers (100 mm)	1.0 ± 0.3	1.6 ± 0.5	225 ± 45	1.80 ± 0.45
SR/PEEK fibers (10 mm)	0.4 ± 0.1	0.9 ± 0.2	156 ± 39	0.70 ± 0.14

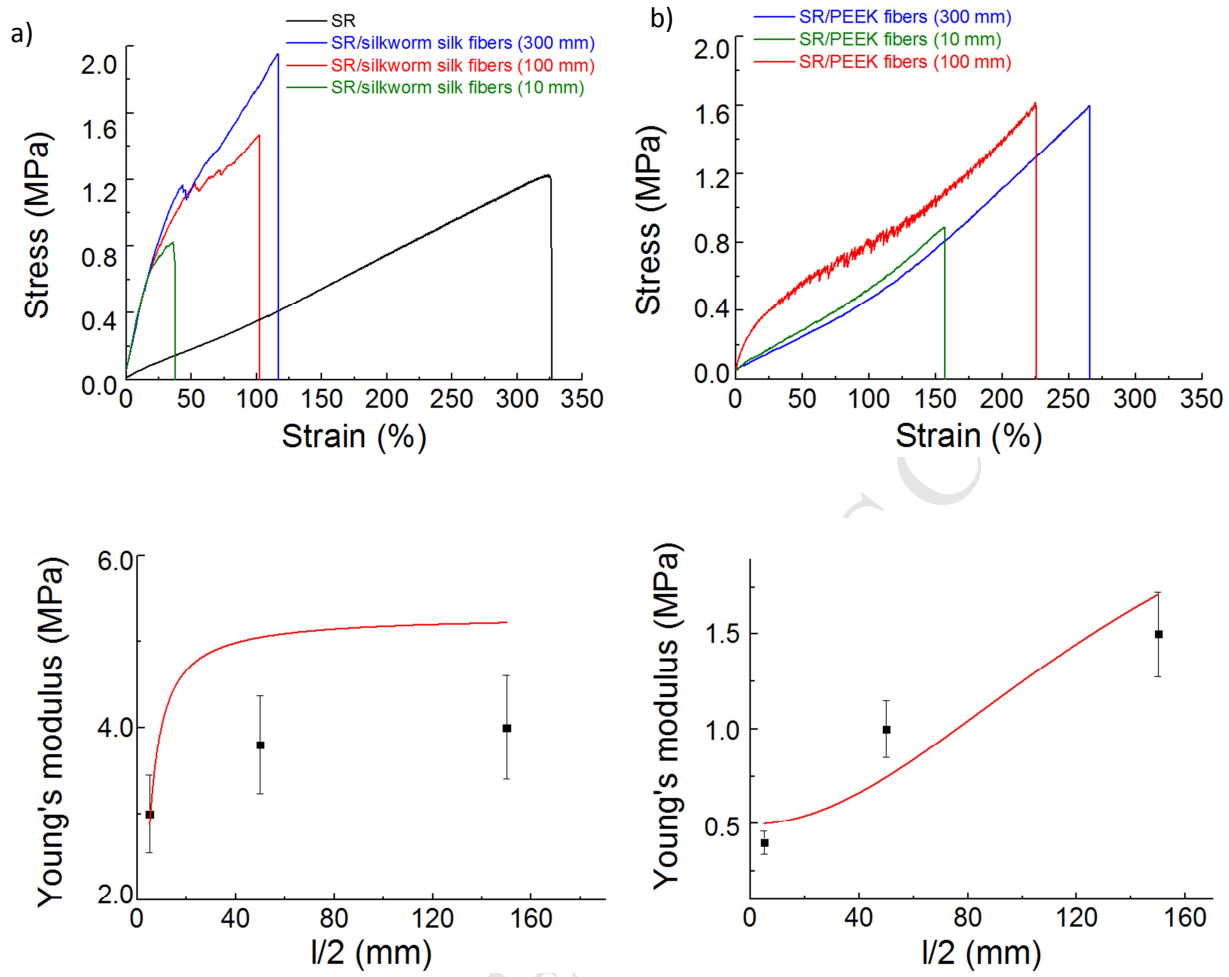

Figure 3. Tensile behaviour and modelling results of (a) SR/silkworm silk fiber composites and (b) SR/PEEK fiber composites vs different fiber length. No best-fitting parameters is considered in the comparison.

Moreover, from a classical direct rule of mixture applied to the data reported in Tab. I, we found that the equivalent strength of the composite filled with 300 mm fiber length was ~ 2.8 MPa (Tab. SI); this is in good agreement with the measured tensile strength of the silk fiber reinforced composite suggesting an efficient stress transfer across the interface from the matrix into the fiber [30].

Silk fiber can be viewed as a semicrystalline nanocompositeswith ordered regions (β-sheet protein nanocrystals) embedded in a softer matrix of disordered material; thus the optical emission property

of the protein nanocrystals are sensitive to the deformation in terms of order or orientation of these domains and thus can be used to determine the strain in the direction of the tensile stress; such optical approach has been adopted to characterize the polymer-fiber interface [19,31,32] where a pigment mixed with the silk fiber was used as fluorescent agent. Representative absorption and emission spectra, where the emitted light was detected using an optical analyzer along the normal to the sample (see experimental setup in Fig. 4a), of SR/silkworm silk fiber composite are shown in Fig. 4b. The luminescence was measured by exciting the samples at 455 nm. It is known that the luminescence is dependent on surrounding environment, thus in order to exclude any contribution from the SR matrix, emission and absorption spectra of the neat matrix were also recorded and reported in the supplementary data section (Fig. S4). From these data we observe both that the SR matrix does not show any Raman shift at the excitation wavelength (i. e. the light is emitted at the same wavelength of the incident beam), and no absorption peak in the emission region of the silk was recorded. Thus we argue that the main contribution to the emission comes from the intrinsic structure of the silk proteins. The silk fibers are made of proteins forming linear sequences that are packed in highly or less ordered crystal regions, i. e. the β-sheets, and can be described by two structural models: Silk I, consisting of β turn, and Silk II, consisting mostly of antiparallel β pleated sheets [33,34]. XRD analysis performed on the unstrained silkworm silk sample (Fig. S5) shows Bragg reflections near $2\theta=9°$ and 20.6° which are the typical signature of native degummed silk with silk II structure [35]. The diffraction pattern registered on the strained sample (Fig. S5) showed the same features indicating that the crystalline spacing of the β-sheets was not altered by the tensile load.

The emission spectra recorded on silkworm silk fiber and silk composite (Figs. 4c and 4d) illustrate some of the characteristic spectral lines of silk fibroin reported by Kaplan et al. [36,37] that it was demonstrated to be sensitive to the β-sheet content. Tensile deformation of silk fibers involves a strong contribution of such stiff phase, presumably in the disordered regions as modelled by Zhou et

al. [38], leading to a luminescence intensity ratio change with increasing the strain on the sample as reported in Figs. 4c and 4d. The luminescence variation could be attributed to the disentanglement of the silk fibers with the strain thus reducing the scattering cross section. This effect has been taken into account by repeating the luminescence on rubber composites fabricated with oriented silk fiber (Fig. S2). We did not observe any emission difference with respect to the random morphology.

The silkworm silk fibers embedded onto the SR matrix emitted a blu light under UV excitation [39] (Fig. 4e), however, the SR matrix remained transparent due to the weak UV excitation of SR. Such different luminescent features between the matrix and the silk fibers significantly improved image resolution for stress transfer visualization (Fig. 4e). In particular, Figure 4e shows the visualization of the silk fibers under UV excitation in response to mechanical strain. Prior to the application of tensile deformation, intrinsic fiber luminescence is visible; during the strain (i. e. $\varepsilon = 0.50$ and 0.70), the luminescent activation of the stress transfer along the fiber is observed.

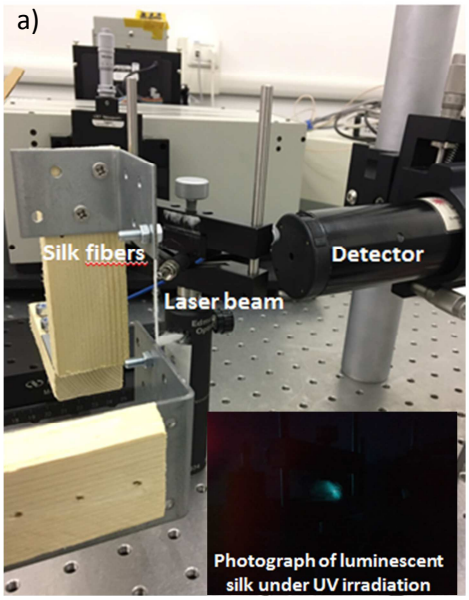
a)
Silk fibers
Detector
Laser beam
Photograph of luminescent silk under UV irradiation

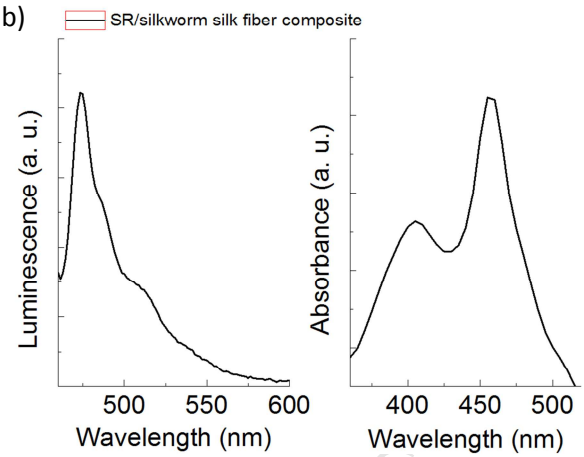
b)
SR/silkworm silk fiber composite
Luminescence (a. u.)
500
550
600
Wavelength (nm)
Absorbance (a. u.)
400
450
500
Wavelength (nm)

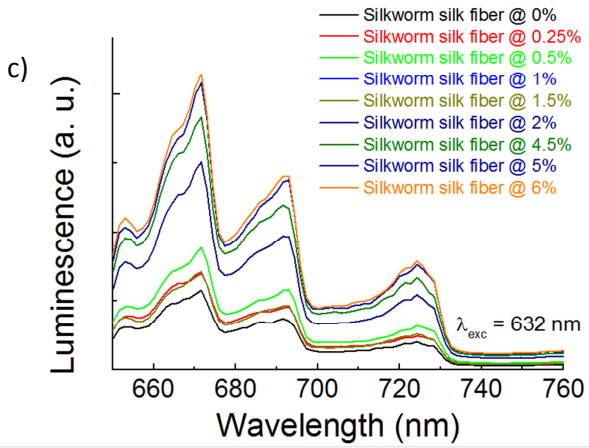
c)
Silkworm silk fiber @ 0%
Silkworm silk fiber @ 0.25%
Silkworm silk fiber @ 0.5%
Silkworm silk fiber @ 1%
Silkworm silk fiber @ 1.5%
Silkworm silk fiber @ 2%
Silkworm silk fiber @ 4.5%
Silkworm silk fiber @ 5%
Silkworm silk fiber @ 6%
Luminescence (a. u.)
λexc = 632 nm
660
680
700
720
740
760
Wavelength (nm)

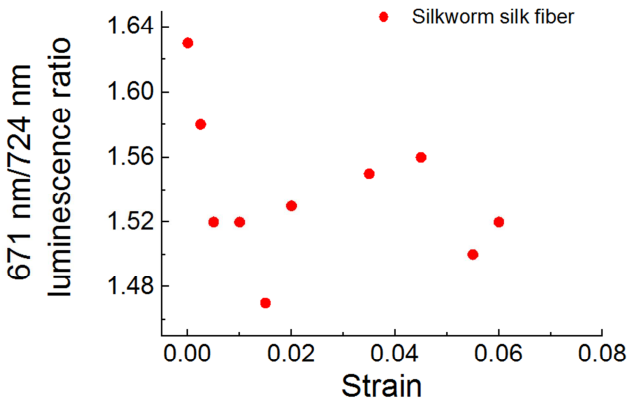
Silkworm silk fiber
671 nm/724 nm luminescence ratio
1.64
1.60
1.56
1.52
1.48
0.00
0.02
0.04
0.06
0.08
Strain

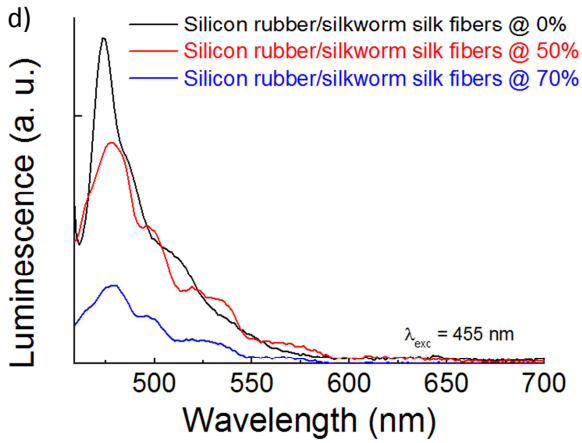
d)
Silicon rubber/silkworm silk fibers @ 0%
Silicon rubber/silkworm silk fibers @ 50%
Silicon rubber/silkworm silk fibers @ 70%
Luminescence (a. u.)
λexc = 455 nm
500
550
600
650
700
Wavelength (nm)

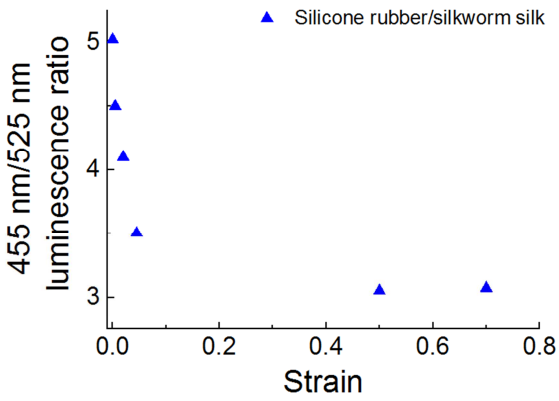
Silicone rubber/silkworm silk
455 nm/525 nm luminescence ratio
5
4
3
0.0
0.2
0.4
0.6
0.8
Strain

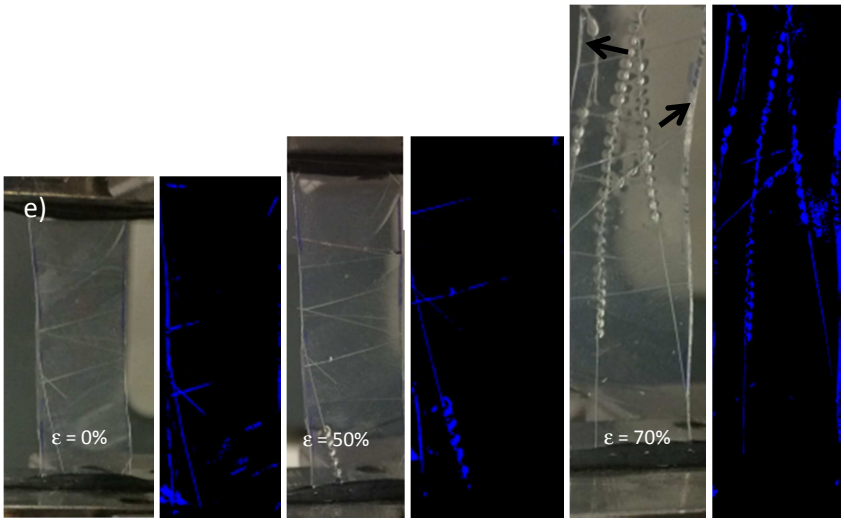

Figure 4. (a) Set-up for luminescence spectra measurement. The inset shows the photograph of luminescent silk mat under UV irradiation. (b) Emission and absorption spectra of SR/silkworm silk fiber composite. (c) Emission spectra of silkworm silk fibers acquired at an excitation of 632 nm and luminescence intensity ratios of silkworm silk fibers at different strains. (d) Emission spectra of silk fiber composite acquired at an excitation of 455 nm and luminescence intensity ratios of silk fiber composite at different strains. (e) The mechanical test and luminescence visualization of stress transfer. Snapshots taken during the uniaxial tensile test on the SR/silkworm silk fiber composite. Rupture event is highlighted by the arrows.

The deformation process was recorded using a tensile machine with a constant strain rate as reported in Fig. 5. The applied strain read from the tensile machine agreed with the strain obtained from direct measurements of the luminescence intensity ratio of the varying distances (Figs. 5a and 5b). Looking at the luminescence pattern, both samples had a uniform deformation that varies linearly at small strains according to the strain measured by the machine. Deviation from this linear behaviour at larger strain was observed and it could be due to sliding from the grips that happen to any stretchable soft polymeric material under tensile tests. Further, the dependence of the sample emission was then recorded under mechanical loading (Fig. 5c). As the silk composite was stretched, the normalized luminescence intensity ratio was found to decrease with the

deformation, reaching a minimum value at λ_{max} (i. e. 2.16). Subsequently, as the specimen was brought to the initial state from λ_{max} to 1, the emission intensity regained the initial values, suggesting an almost reversible mechanism.

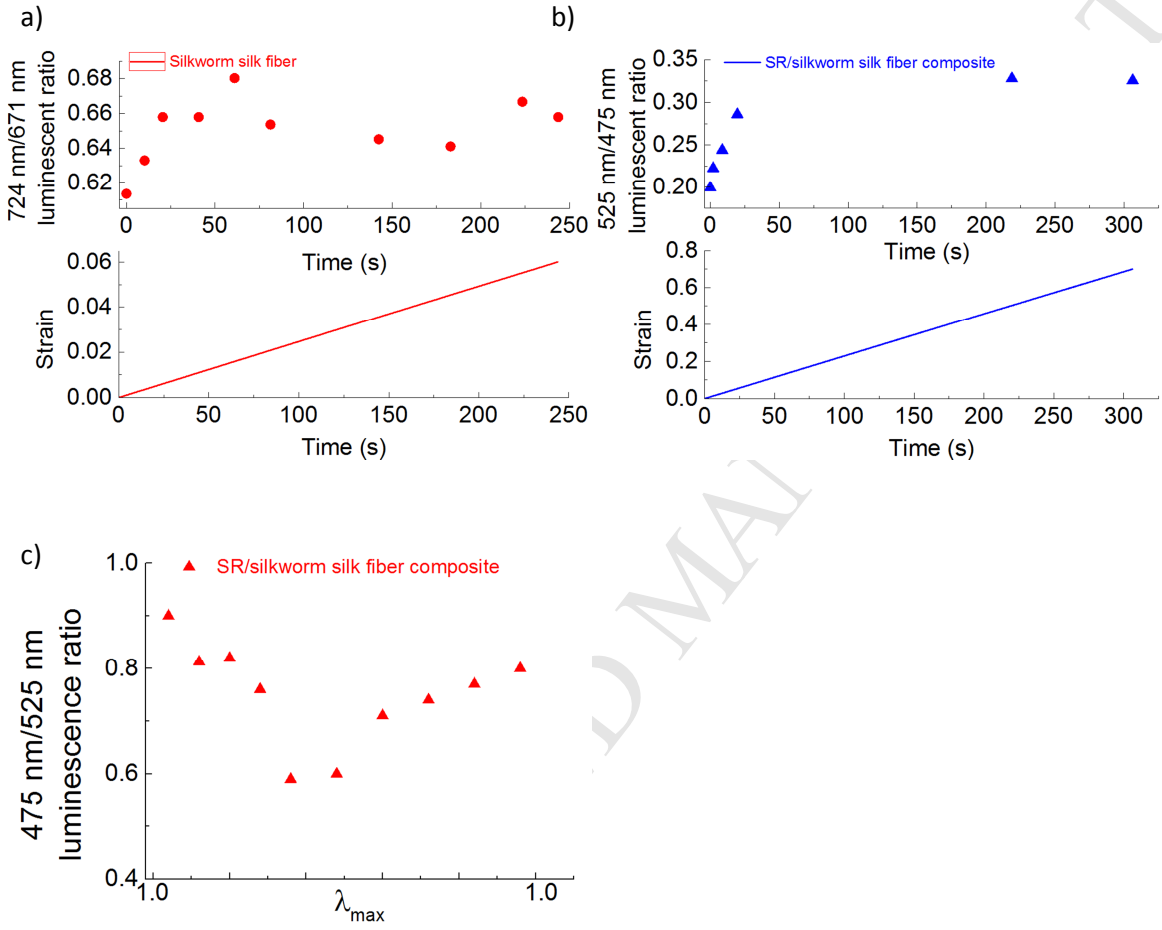

Figure 5. Luminescence intensity ratio as a function of time compared against the applied deformation by tensile machine for (a) silkworm silk fiber and (b) SR/silkworm silk fiber composite. (c) Variations of the luminescence intensity ratio to initial value of SR/silkworm silk fiber composite through the stretching cycles from λ=1 to λ_{max}=2.16, then returned to a relaxed state ($\lambda_{max} \rightarrow 1$).

Conclusions

Insertion of silkworm silk fibers in a stretchable rubbery matrix was found to be a powerful, yet simple system for predicting the composite stiffness and probing the strain with luminescent emission of the silk patterns in the composite. The advantages of this system include the commercial availability of the fibers, silkworm silk, and the simple composite casting method by polyaddition of commercial silicone rubber. The degummed silk strands were found stiffer than monofilament PEEK fibers. Using the luminescence pattern of silk fibers materials we realize an optical strain gauge. We show that such a strain gauge can measure the deformation by using the intensity ratio of the emission spectra and our measurements reflect the material deformation measured by universal tensile machine. We expect our results can be extended to obtain strain sensors to monitor the nonlinear constitutive laws of polymeric with real-time measurements. Moreover, these silk based strain gauges would have the potential for in situ strain measurements of soft tissues, which might be used to characterize the biomechanical function of biological tissues.

Acknowledgments

NMP is supported by the European Commission H2020 under the Graphene Flagship (WP14 “Polymer composites”, n. 696656) and under the FET Proactive (“Neurofibres” no. 732344). Prof. Miguel-Angle Lopez-Manchado (Instituto de Ciencia y Tecnología de Polímeros, ICTP-CSIC, Madrid) is kindly acknowledged for the XRD analysis.

References

[1] G. H. Altman, R. L. Horan, H. H. Lu, J. Moreau, I. Martin, J. C. Richmond, D. L. Kaplan, Silk matrix for tissue engineered anterior cruciate ligaments, Biomaterials 23 (2002) 4131-4141.

[2] G. H. Altman, H. H. Lu, R. L. Horan, T. Calabro, D. Ryder, D. L. Kaplan, P. Stark, I. Martin, J. C. Richmond, G. Vunjak-Novakovic, Advanced bioreactor with controlled application of multi-dimensional strain for tissue engineering, J Biomech Eng 124 (2002) 742-749.

[3] H.J. Jin, J. Park, R. Valluzzi, P. Cebe, D.L. Kaplan, Biomaterial films of Bombyx mori silk fibroin with poly[ethylene oxide], Biomacromolecules 5 (2004) 711-717.

[4] U. J. Kim, J. Park, C. Li, H. J. Jin, R. Valluzzi, D. L. Kaplan, Structure and properties of silk hydrogels, Biomacromolecules 5 (2004) 786-792.

[5] R. Nazarov, H.J. Jin, D.L. Kaplan, Porous 3-D scaffolds from regenerated silk fibroin, Biomacromolecules 5 (2004) 718-726.

[6] H. V. Danks, The roles of insect cocoons in cold conditions, Eur. J. Entomol. 101 (2004) 433-437.

[7] H.-P. Zhao, X.-Q. Feng, S.-W. Yu, W.-Z. Cui, F.-Z. Zou, Mechanical properties of silkworm cocoons, Polymer 46 (2005) 9192-9201.

[8] A. Woesz, J. Stampfl, P. Fratzl, Cellular solids beyond the apparent density–an experimental assessment of mechanical properties, Adv. Eng. Mater. 6 (2004) 134–8.

[9] J. Perez-Rigueiro, M. Elices, J. Llorca, C. Viney, Effect of degumming on the tensile properties of silkworm [Bombyx mori] silk fiber, J. Appl. Polym. Sci. 84 (2002) 1431–1437.

[10] P. Poza, J. Perez-Rigueiro, M. Elices, J. Llorca, Fractographic analysis of silkworm and spider silk, Eng. Frac. Mech. 69 (2002) 1035–1048.

[11] M. A. Sawpan, K. L. Pickering, A. Fernyhough, Effect of fibre treatments on interfacial shear strength of hemp fibre reinforced polylactide and unsaturated polyester composites, Composites Part A: Applied Science and Manufacturing 42 (2011) 1189-1196.

[12] S. Keten, Z. Xu, B. Ihle, M. J. Buehler, Nanoconfinement controls stiffness, strength and mechanical toughness of β-sheet crystals in silk, Nature Materials 9 (2010) 359–367..

[13] S. Ling, Q. Zhang, D. L. Kaplan, F. Omenetto, M. J. Buehler, Z. Qin, Printing of stretchable silk membranes for strain measurements, Lab on a Chip 16 (2016) 2459–2466..

[14] V. Benfenati, S. Toffanin, R. Capelli, L. M. Camassa, S. Ferroni, D. L. Kaplan, F. G. Omenetto, M. Muccini, R. Zamboni, A silk platform that enables electrophysiology and targeted drug delivery in brain astroglial cells, Biomaterials 31 (2010) 7883-7891.

[15] V. Benfenati, K. Stahl, C. Gomis-Perez, S. Toffanin, A. Sagnella, R. Torp, D. L. Kaplan, G. Ruani, F. G. Omenetto, R. Zamboni, M. Muccini, Biofunctional silk/neuron interfaces, Adv. Fun. Mater. 22 (2012) 1871-1884.

[16] S.-W. Hwang, X. Huang, J.-H. Seo, J.-K. Song, S. Kim, S. Hage-Ali, H.-J. Chung, H. Tao, F. G. Omenetto, Z. Ma, J. A. Rogers, Materials for bioresorbable radio frequency electronics, Adv. Mater. 25 (2013) 3526-3531.

[17] H. Ito, T. Saito, N. Oshima, N. Kitamura, S. Ishizaka, Y. Hinatsu, M. Wakeshima, M. Kato, K. Tsuge, M. Sawamura, Reversible Mechanochromic Luminescence of [(C6F5Au)2(μ-1,4-Diisocyanobenzene), J. Am. Chem. Soc. 130 (2008) 10044–10045.

[18] N. Terasaki, C. Li, L. Zhang, C.-N. Xu, Active crack indicator with mechanoluminescent sensing technique, Sensors Journal IEEE 13, (2013) 3999-4004.

[19] W. J. Woodcock, R. Beams, C. S. Davis, N. Chen, S. J. Stranick, D. U. Shah, F. Vollrath, J. W. Gilman, Observation of interfacial damage in a silk-epoxy composite, using a simple mechanoresponsive fluorescent probe, Adv. Mater. Interfaces 4 (2017) 1601018.

[20] H. Krenchel, Fiber Reinforcement, Akademisk Forlag, Copenhagen [1964].

[21] C. C. Rusa, C. Bridges, S.-W. Ha, A. E. Tonelli, Conformational changes induced in Bombyx mori silk fibroin by cyclodextrin inclusion complexation, Macromolecules 38 (2005) 5640–5646.

[22] E. S. Sashina, G. Janowska, M. Zaborski, A.V. Vnuchkin, Compatibility of fibroin/chitosan and fibroin/cellulose blends studied by thermal analysis, J. Therm. Anal. Calorimet. 89 (2007) 887–891.

[23] H. Y. Kweon, I. C. Um, Y. H. Park, Structural and thermal characteristics of Antheraea pernyi silk fibroin/chitosan blend film, Polymer 42 (2001) 6651–6656.

[24] Z. Shao, F. Vollrath, Materials: Surprising strength of silkworm silk, Nature 418 (2002) 741.

[25] L. J. Gibson, M. F. Ashby, The mechanics of three-dimensional cellular materials, Proc. R. Soc. London, Ser. A 382 (1982) 43-51.

[26] F. Chen, D. Porter, F. Vollrath, Structure and physical properties of silkworm cocoons, J. R. Soc. Interface 9 (2012) 2299–2308.

[27] J. L. Thomason, The influence of fiber length and concentration on the properties of glass fiber reinforced polypropylene, Composites Part A: Applied Science and Manufacturing 27 (1996) 477-484.

[28] J. A. Rosenthal, Model for determining fiber reinforcement efficiencies and fiber orientation in polymer composites, Polym. Compos. 13 (1992) 462-466.

[29] R. Gibson, Principles of Composite Material Mechanics, McGraw-Hill, New York [1994]

[30] K.L. Pickering, M.G. Aruan Efendy, T.M. Le, A review of recent developments in natural fibre composites and their mechanical performance, Composites Part A: Applied Science and Manufacturing 83 (2016) 98-112.

[31] Z. Shao, R. J. Young, F. Vollrath, The effect of solvents on spider silk studied by mechanical testing and single-fiber Raman spectroscopy, Int. J. Biol. Macromol. 24 (1999) 295–300.

[32] I. Georgakoudi, I. Tsai, C. Greiner, C. Wong, J. DeFelice, D. L. Kaplan, Intrinsic fluorescence changes associated with the conformational state of silk fibroin in biomaterial matrices, Optics Express 15 (2007) 1043–1053.

[33] X. Hu, D. L. Kaplan, P. Cebe, Determining beta-sheet crystallinity in fibrous proteins by thermal analysis and infrared spectroscopy, Macromolecules 39 (2006) 6161–6170.

[34] T. Asakura, K. Ohgo, T. Ishida, P. Taddei, P. Monti, R. Kishore, Possible implications of serine and tyrosine residues and intermolecular interactions on the appearance of silk I structure of Bombyx mori silk fibroin-derived synthetic peptides: high-resolution 13C cross-polarization/magic-angle spinning NMR study, Biomacromolecules 6 (2005) 468–474.

[35] F. Zhang, X. You, H. Dou, Z. Liu, B. Zuo, X. Zhang, Facile fabrication of robust silk nano fibril films via direct dissolution of silk in CaCl2 − formic acid solution, ACS Appl. Mater. Interfaces 7 (2015) 3352−3361.

[36] H. J. Jin, D. L. Kaplan, Mechanism of silk processing in insects and spiders, Nature 424 (2003) 1057–1061.

[37] W. L. Rice, S. Firdous, S. Gupta, M. Hunter, C. W. P. Foo, Y. Wang, H. J. Kim, D. L. Kaplan, I. Georgakoudi, Non-invasive characterization of structure and morphology of silk fibroin biomaterials using non-linear microscopy, Biomaterials 29 (2008) 2015–2024.

[38] H. Zhou, Y. Zhang, Hierarchical chain model of spider capture silk elasticity, Phys. Rev. Lett. 94 (2005) 028104.

[39] N. C. Tansil, Y. Li, C. P. Teng, S. Zhang, K. Y. Win, X. Chen, X. Y. Liu, M.-Y. Han, Intrinsically colored and luminescent silk, Adv. Mater. 23 (2011) 1463–1466.